One-step fabrication of biomimetic PVDF-$BaTiO_3$ nanofibrous composite using DoE

Dinesh Ramesh[1], **Nandika Anne D'Souza**[1,2]

[1]Mechanical and Energy Engineering, University of North Texas, Denton, Texas, USA
[2]Materials Science and Engineering, University of North Texas, Denton, Texas, USA

E-mail: mail2dineshram@gmail.com

Abstract.

Dielectric polyvinylidene fluoride (PVDF) and Barium titanate ($BaTiO_3$)-PVDF nano-fibrous composites were made using the electrospinning process based on a design of experiments approach. An ultrasonication process was optimized using 2^k factorial DoE approach to disperse $BaTiO_3$ particles in PVDF solution in DMF. Scanning electron microscopy was used to characterize the microstructure of the fabricated mesh. The FT-IR and Raman analysis were carried out to investigate the crystal structure of the prepared mesh. Surface morphology contribution to the adhesive property of the composite was explained through contact angle measurements. The capacitance of the prepared PVDF-$BaTiO_3$ nanofibrous mesh was over 40 % than the pure PVDF nanofibers. The results obtained indicates that electrospinning offers a potential way to produce nanofibers with desired crystalline nature which was not observed in molded samples. In addition, $BaTiO_3$ can be used to increase the capacitance, desired surface characteristics of the PVDF nanofibers which can find potential application as flexible piezoelectric sensor mimicking biological skin for use in structural health monitoring applications.

Keywords: Polyvinylidene fluoride (PVDF), Barium titanate ($BaTiO_3$), Ultrasonication, Electrospinning, Design of Experiments (DoE).

1. Introduction

The functional properties of the polymer can be tailored by adding reinforced filler, varying filler composition, filler particle size, processing conditions etc., [1, 2]. The incorporated fillers can be 0-Dimensional quantum dots [3], 1-Dimensional nanotubes [4], 2-Dimensional layered materials [5]. PVDF is a thermoplastic ferroelectric polymer, having higher dielectric constant(κ) values, above 10, because of its polar backbone [6] and can be used for making flexible piezoelectric materials. The piezoelectric property of the polymer can be increased by adding piezoelectric ceramic fillers such as TiO_2, $PbZrO_3$ (PZT) and $BaTiO_3$ and these flexible piezoelectric polymer-ceramic composites are attractive materials for various applications such as embedded membrane sensors [7, 8, 9] for structural health monitoring applications [10]. In this work, $BaTiO_3$ was chosen due to the piezoelectric property over TiO_2 and lower toxicity compared to PZT.

$BaTiO_3$ of varying size/content can be added to improve the structural and functional properties of the host PVDF matrix [11]. The improvement in dielectric properties of host PVDF with $BaTiO_3$ nanoparticles were previously reported [12]. However, the nano sized $BaTiO_3$ particles tend to dissipate the energy due to high amount of charge carriers present in the structure and this effect contributes to a large hystersis loop as reported in [9]. As the particle size increases, the hysteresis loop becomes narrow. This is because, when an electric field is appiled, the large amount of charge carriers/ionic defects present in the particles in the range of 10 - 50 nm move along the electric field resulting in dissipation of energy. To have a high capacitance, the material should be able to store charges without dissipating and hence a large particle size filler was envisioned. Further, the d_{33} values of $BaTiO_3$ depends on the grain size and processing route. The obtained $BaTiO_3$ powders consists of aggregated, irregular and micron-sized particles morphology with average grain size of approx. 3 μm [13]. It is to be noted that the average value of d_{33} for of 3 μm $BaTiO_3$ particles is in the range of 250-300 pC/N [14] and the maximum dielectric constant (ε) value for obtained $BaTiO_3$ was reported to be 470 [13]. In this work, the < 3 μm $BaTiO_3$ particles obtained from Sigma-Aldrich was used as ceramic filler with PVDF for improving the capacitance of the host PVDF polymer matrix.

In addition, the interfacial adhesion property is one of the challenges faced by flexible sensors. To improve the adhesion property of the material with the electrode, tuning of microstructural morphology is required, which in turn improves the interfacial adhesion and thereby sensing property. Preparing a nanofibrous membrane, can help in making a structure which mimics the Gecko feet morphology [15]. Electrospinning has been extensively explored for generating continuous long polymer fibers from micro to nanoscale range by the application of electrostatic forces to a jetting polymer solution. The combinatorial approach of electrospinning/3D printing offers numerous advantages in fabricating multiscale complex structures [16]. The major challenge involved in the fabrication process is the formulation of electrospinning solution.

When polymer ceramic composite materials with large filler particle size are

prepared, the dispersion of ceramic particles may not be uniform and for making the electrospinning solution, the added ceramic particles should be well dispersed in solution. Due to the strong electrostatic force, the $BaTiO_3$ particles tend to agglomerate in solution. The agglomeration of added fillers affects the electrospinning process, resulting in electrosprayed materials with particle morphology instead of fibrous morphology. The stability of the dispersed particles in solution depends on the choice of solvent and dispersing method. Ultrasonication can aid in dispersing the polar ceramic particles in the polymer solution. Therefore, a fine tuning of filler concentration and ultrasonication of solution is required to get the desired viscosity for electrospinning process. To get the desired viscosity of the solution, trial and error method is followed, which is time consuming and expensive.

Design of experiments (DoE) is a simple and effective way to reduce the time and cost of experimental trials for optimizing the process and get the desired output. In this work, 2^k factorial design approach was used to optimize electrospinning solution's viscosity with ≤ 3 μm $BaTiO_3$ particles with PVDF to assess the feasibility of electrospinning process yielding polymer fibrous morphology. The aim of this paper is 2-fold, 1. In-situ fabrication of PVDF-$BaTiO_3$ biomimetic flexible nanofibrous composite mesh fibers by electrospinning process using DoE, and 2. The morphology and crystal structure characterization, and correlating with the material's structure property relationship for improving surface adhesion property.

2. Material and Methods

2.1. Material

Polyvinylidene fluoride (PVDF) was obtained in powder form from Sigma-Aldrich (CAS Number 24937-79-9) with average molecular weight of $\sim$ 534,000 (Mw). The density is 1.74 g/mL at $25°C$ and refractive index is 1.43 (n20/D). $BaTiO_3$ (FW 233.24) was obtained in powder form from Sigma-Aldrich (CAS Number 12047-27-7). The average particle size is < 3 micron with the purity of 99 %. The density of the powder is 6.08 g/cc at $25°C$. N, N-Dimethylformamide (DMF) (MW 73.09 g/mol) CHROMASOLV® Plus, for HPLC, $\geq$ 99.9% was purchased from Sigma-Aldrich (CAS Number 68-12-2). DMF was used as a solvent for dissolving PVDF and dispersing ceramic particles.

2.2. Fabrication

The solvent used in electrospinning process also plays an important role in electrospinnablity of the solution, therefore it is important to use an appropriate solvent that can dissolve the polymer and is at the same time electrospinnable [17]. A highly viscous solution and therefore the polymer concentration is desired to make a stable dispersion of particles. Solvents such as N, N-Dimethylformamide (DMF) and N-methyl pyrrolidinone (NMP) are widely used for making electrospinning solution. In this work,

DMF was used as a solvent for dissolving PVDF and dispersing ceramic particles to make an electrospinning suspension.

A 13% (w/w) PVDF solution in DMF was be made using magnetic stirrer in a 250 mL beaker at 700 rpm (rotation per min for 30 min). The beaker was covered with a lid to avoid evaporation of the solvent. The maximum solubility of the PVDF polymer in DMF was found to be 13% (w/w) at room temperature. Any amount of polymer beyond 13% (w/w) resulted in insoluble polymer material floating in the solution. The solubility of the polymer can be further improved by dissolving at a higher temperature of about 50°C. However, to avoid degradation of the polymer material, it was dissolved in the solvent at room temperature.

Ultrasonication was performed to disperse the $BaTiO_3$ particles (3% (w/w) with respect to polymer) in the polymer solution. A Sonic vibracell was used for this purpose. The pulse amplitude was set at 25%. The $BaTiO_3$ particles were dispersed in polymer solution in DMF for the duration of 40 min with 5 min interval. The pulse rate was 10 seconds of ultrasonication treatment followed by 1 sec halt. During ultrasonication, the entire solution was kept in a water bath to avoid overheating due to ultrasonication which will result in evaporation of the solvent and to avoid degradation of the polymer solution due to overheating [18]. A 5 mL of this electrospinning solution was taken in a syringe and used for electrospinning.

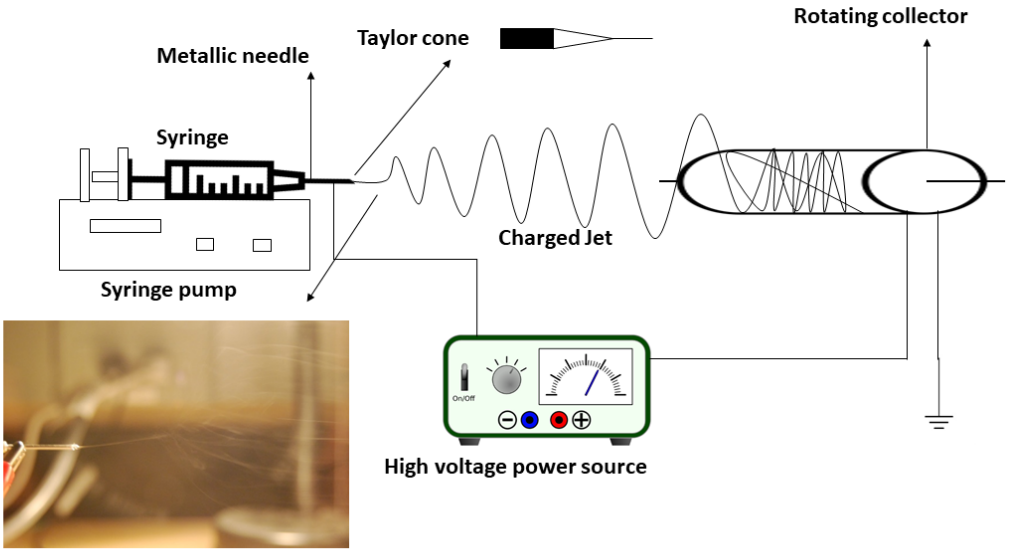

Figure 1: Schematic of electrospinning setup.

The electrospinning setup consists of three parts: voltage generator, syringe pump and spinning collector (see Figure 1). The syringe pump is used for injecting the polymer solution via a needle (18" Gauge, 1.5") purchased from Vita needles. The voltage

Table 1: 2^k factorial design approach with four levels and two parameters (Ultrasonication duration and Filler ($BaTiO_3$-3%) concentration in percent.)

Four levels	Filler concentation (%)	Ultrasonication duration (min.)
-,-	1	5
+,-	5	5
-,+	1	60
+,+	5	60

generator creates an electric field between the tip of the needle and the aluminum foil on the collector. The voltage applied was 20 kV. The distance between the tip of the needle and collecting roller was kept at 15 cm. Due to the applied voltage the fibers were drawn from the solution and adsorbed on to the non-stick aluminum foil rolled on to the roller rotating at 400 rpm. The purpose of using the roller was to get aligned/oriented fibers as compared to a plate collector.

3. Design of Experiments (DoE)

A Design of Experiments approach was successfully used for optimizing electrospun fiber morphology using response surface methodology [19], orthogonal experimental design [20], factorial design [21] etc., The 2^k factorial design approach was chosen, with two factors (filler concentration and ultrasonication duration) and each factor has two levels (-,+). The - level indicates lower level and + indicates upper level leading to four levels as indicated in Table 1.

A total of 16 process parameters combinations, including four replicates of middle point, were generated. The value of 1 was assigned for the results with electrospray morphology as the outcome of the experiment and the value of 2 was assigned for electrospinning fibrous morphology as the outcome of the experiment. The statistical analysis was carried out using R-Package [22, 23]. The other process parameters including, applied voltage, distance between needle and the collector, rotor speed were optimized for electrospinning PVDF nanofibers. The same conditions were used for making the composite as well. The two vital parameters of filler concentration and ultrasonication duration were chosen designing experiments. Based on the experimental results and DOE analysis from Figure 2, an optimum solution of 3 % filler concentration and an ultrasonication duration of 40 min were selected to optimize the electrospinning solution for making nanofibrous composite.

4. Characterization

For electron microscopy and EDS (Energy dispersive X-ray spectroscopy) analysis, the sample surface was metallized using (60/40) Pd/Au alloy [24] using sputtering. A Model 5100 from POLARON instruments Inc. was used to sputter the sample. The Ar ion

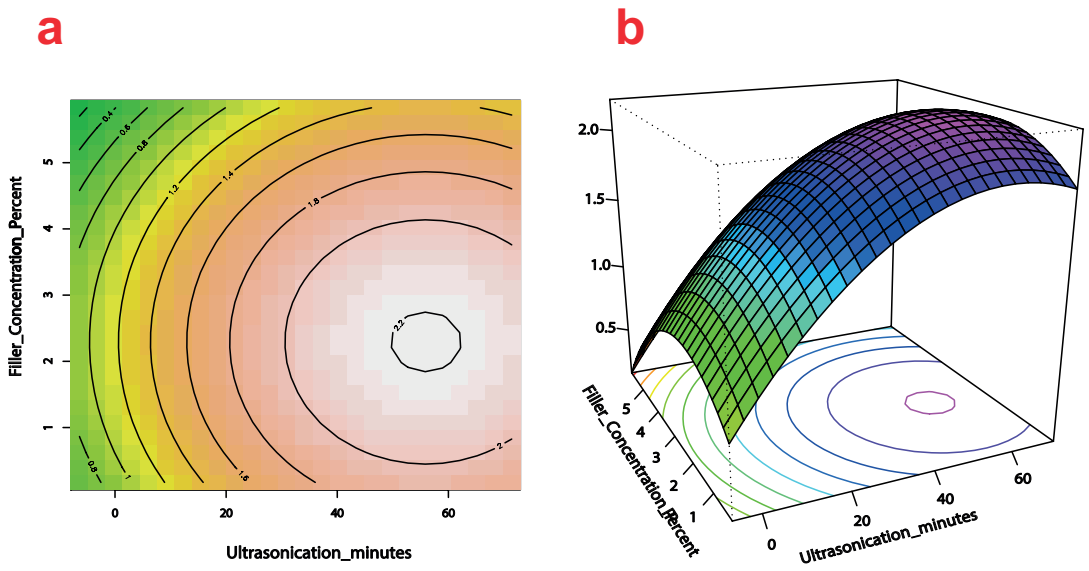

Figure 2: Response surface plots by DoE a) Contour plot, b) 3D Perspective

plasma was used for sputtering. The voltage and current were set at 2.5 kV and 5 mA. The plasma was initiated at 20 mA current and sustained for 4 min to coat a thin layer of metallic film to prevent surface "charging" and to protect the sample surface from e-beam induced damage.

The morphology of the collected nanofibrous mesh was characterized using Scanning electron microscope (SEM). A FEI-Quanta Environmental SEM was used to get the lateral image of fibers. The analysis was carried out at low vacuum using a 15 kV beam current and 5.0 nm spot size. The diameter of the fibers were measured from the SEM pictures using Image J [25]. Contact angle measurements were carried out by a static sessile drop technique using a CAM-Plus® Contact Angle Goniometer (Cheminstruments, Inc., Fairfield, OH), equipped with a fiber optic light source. The measurement was based on the patented half angle method (US Patent 5 268 733) which eliminates the errors associated with arbitrary tangential alignment.

The FT-IR analysis was carried out using a Nicolet IR spectrometer. The samples were analyzed in an attenuated total reflectance (ATR) detector over a 600-1600 cm^{-1} wavelength range by placing the sample on diamond crystal of a known refractive index at a resolution of 4 cm^{-1} over 32 scans.

Raman scattering measurement was performed using Almega XR Raman spectrometer. A 532 nm wavelength was used as the excitation laser source with a spectral resolution of 2 cm^{-1} full width half maximum (FWHM) (1 cm^{-1} per CCD pixel element). The scanning wavelength range was from 200 cm^{-1} to 4000 cm^{-1}. For illustrative purpose of beta phase formation with electrospinning process compared to compression molding, Raman spectra with a range from 775 cm^{-1} to 865 cm^{-1} were also conducted.

A TA instrument ARES strain controlled shear rheometer and an Agilent E4980A

multimeter were used to test dielectric permittivity of the samples. Samples were cut into 25 mm (diameter) circular parallel plate geometry for analysis. During the test, the temperature was maintained at 25°C. To prevent the piezoelectric effects, no axial force was applied to sample. For the frequency scan test, Agilent E4980A multimeter applies 1V DC voltage to sample. The frequency of the electrical field was scanned from 20 Hz to 2 MHz. The obtained dielectric perimittivity values were used to calculate the capacitance of the electrospun mats.

5. Results and Discussion

5.1. Morphology

The morphology of the electrospun fibers are shown in Figure 3. Electrospinning involves stretching of the electrospinning solution caused by the repulsion of charges at its surface [26]. The charges on the polymer should be high enough to overcome the surface tension of the solution. As the solution jet accelerates from the tip of the source to the rotating collector, the solution is stretched while surface tension of the solution may cause the solution to breakup into droplets [27]. Hence highly charged materials like PVDF aid in efficient formation of nanofibers.

The viscosity of polymer solution has a profound effect on electrospinning and the resultant fiber morphology [28, 29]. The molecular weight of the polymer represents the polymer chain length which in turn has an effect on viscosity. Applied voltage has a direct effect on stretching and acceleration of the polymer jet. At lower voltage, the reduced acceleration of jet may increase flight time and may favor the formation of finer fibers with better crystalline structure [30]. At higher voltage, it is found that a greater tendency of bead formation [31]. The applied voltage was optimized at 20 kV to get a finer fibrous mesh. The internal diameter of the needle has a certain effect on the electrospinning process. A smaller internal diameter found to reduce the clogging as well as the amount of beads on the surface of the fiber [32]. The microscopic observation from SEM picture, validates the nanofibers formation in electrospinning process. The average diameter of the fibers of PVDF-$BaTiO_3$ composite was $\approx$ 250 nm compared PVDF nanofibers which is $\approx$ 800 nm. This decrease in fiber diameter can be attributed to the agglomeration of fine $BaTiO_3$ particles in the solution resulted from ultrasonication. Micron sized metal oxide powders such as $BaTiO_3$ consists of particles that exhibit weak Van der Waals forces and strong chemical forces which makes the particles held together as agglomerates. Ultrasonication causes de-agglomeration, resulting in breaking of micron-sized particles exposing new surface area. The resulting fine particles will now have more surface area per unit volume showing a high affinity for agglomeration [33] and tend to agglomerate in solution. This re-agglomeration of $BaTiO_3$ particles causes an emulsion type solution. The emulsion is less viscous than the pure polymer solution. This slight decrease in viscosity of the solution yields fine nanofibrous composite mesh compared to pure PVDF nanofibers.

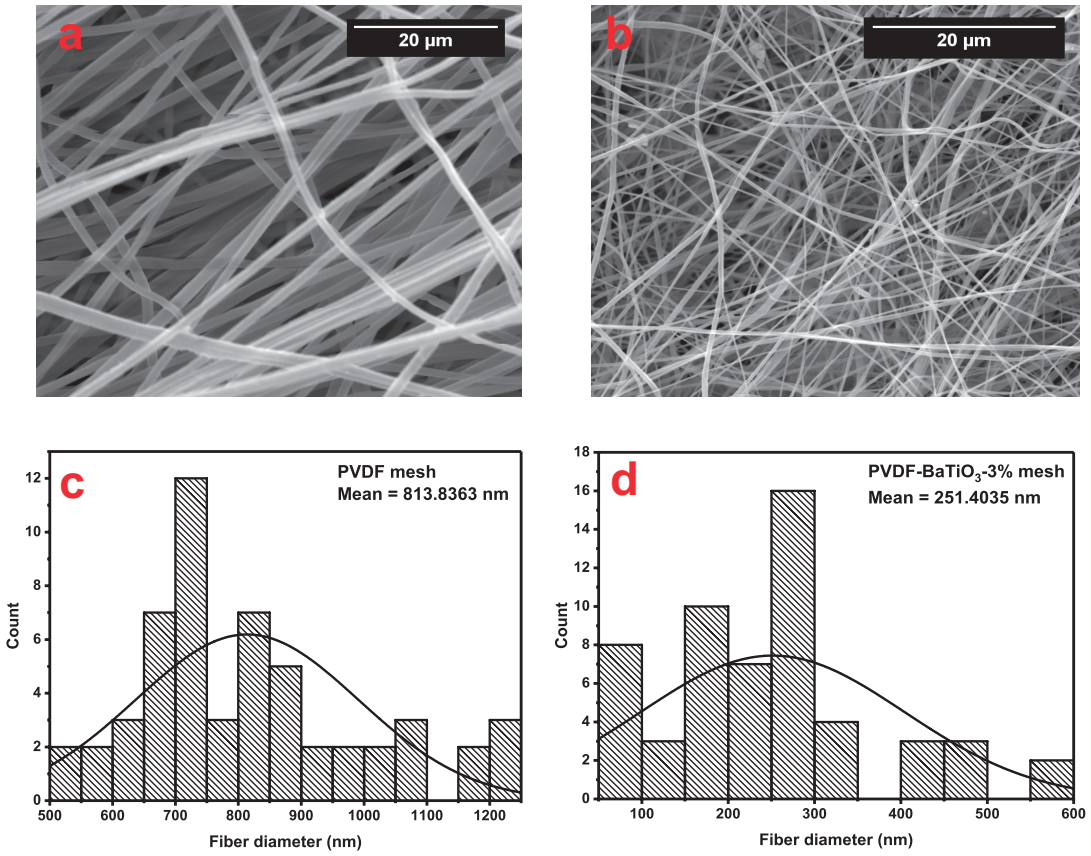

Figure 3: Scanning electron microscopy of a) electrospun PVDF nanofibers, b) electrospun PVDF-$BaTiO_3$-3% nanofibrous composite c) Average fiber diameter for electrospun PVDF and d) electrospun PVDF-$BaTiO_3$-3% nanofibrous composite

The energy dispersive X-ray spectroscopy (EDS) was used for qualitative analysis of PVDF nanofibers and PVDF-$BaTiO_3$ nanofibrous composite mesh to validate the presence of $BaTiO_3$ particles in the composite. The results are shown in the Figure 4. Ba, Ti and O peaks were identified in the composite sample 4b compared to PVDF 4a where C and F peaks are present. The Pd and Au peaks came from the sputter coated thin conducting film that was used to prevent surface charging.

5.2. Barium titanate phase by phonon analysis

$BaTiO_3$ exists in five different polymorphs including hexagonal, cubic, tetragonal, orthorhombic, and rhombohedral crystal structure. Except cubic phase all other phases exhibit ferroelectricity. The room temperature phase is tetragonal. The origin of spontaneous polarization in tetragonal phase in the absence of applied field can be explained on the basis of distortion in crystal structure. The obtained $BaTiO_3$ powder (CAS Number 12047-27-7) from sigma-aldrich has tetragonal structure as confirmed by XRD measurements [34]. The Raman spectra provided by the manufacturers also matches with tetragonal structure.

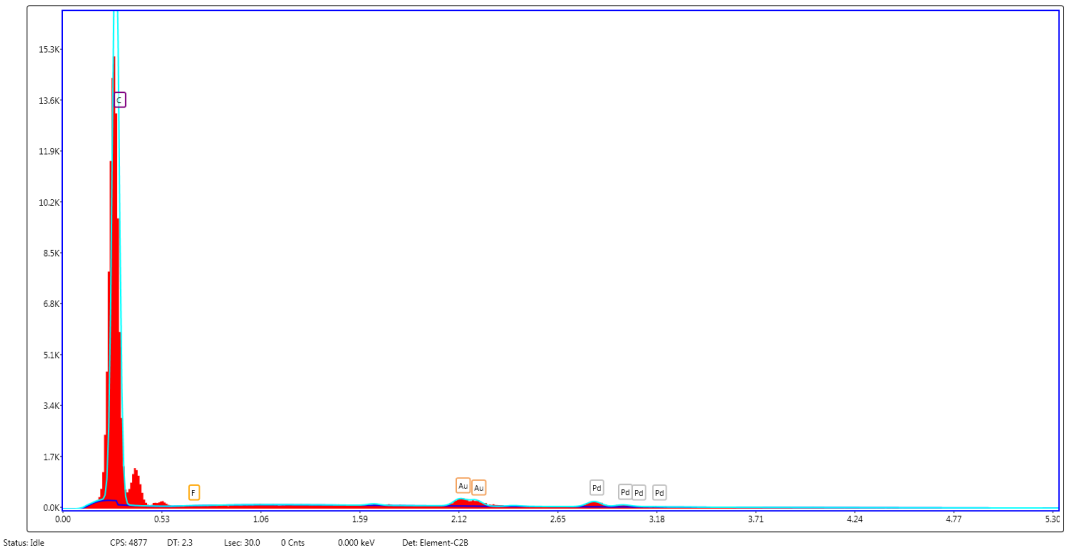

(a) PVDF nanofibers.

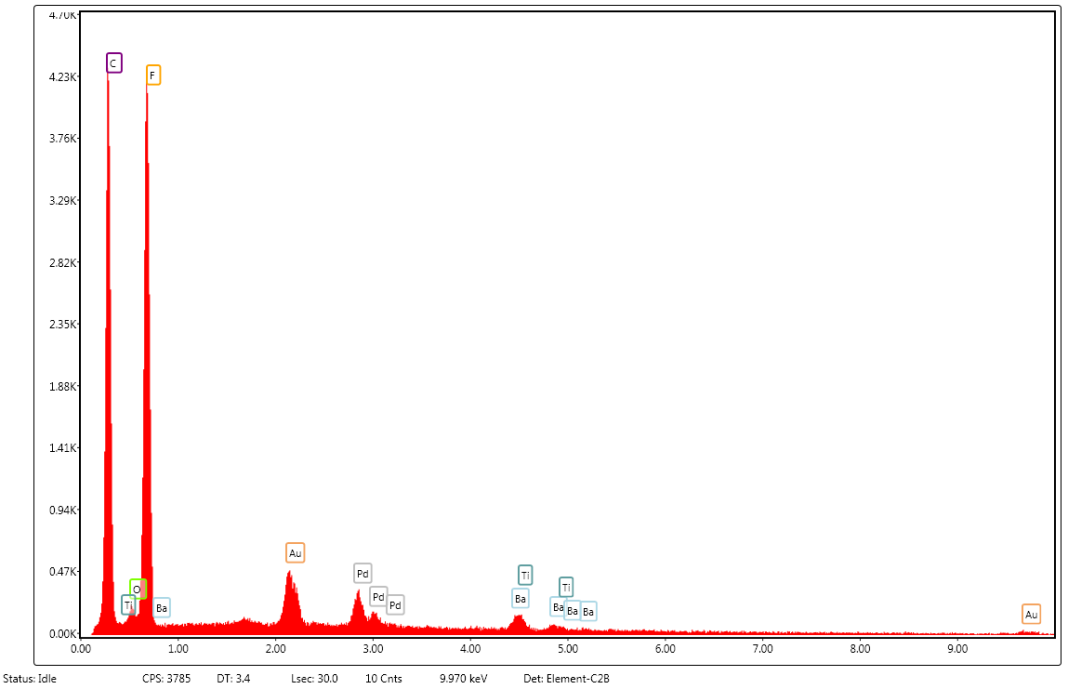

(b) PVDF-$BaTiO_3$-3% nanofibrous composite.

Figure 4: Qualitative EDS analysis analysis of PVDF nanofibers and PVDF-$BaTiO_3$-3% nanofibrous composite.

The tetragonal structure is distorted perovskite where a and b are equal and c length being different with c/a ratio of 1.011. Since the tetragonal $BaTiO_3$ has small c/a ratio of 1.011, accurate determination of lattice constant and thereby phase identification by powder X-ray diffraction and electron diffraction measurements prove to be difficult due to line broadening effect [35]. This line broadening effect can be a result of combined effect of crystallite size, fibrous morphology, non-uniform strain in the material and instrumental broadening. Phonon analysis by Raman scattering has a better resolution of bond length and angle between cation and anion and expected to have better resolution than X-ray and electron diffraction methods. So, Raman analysis was carried out for the phase identification of $BaTiO_3$ in the nanofibrous composite. Raman active modes for tetragonal $BaTiO_3$ are $4E(TO+LO)+ 3A_1(TO+LO) + 1B_1(TO+LO)$, at room temperature. At curie temperature of about $\approx 120°C$, $BaTiO_3$ is expected to undergo order-disorder type phase transition [36] to cubic phase ($Pm\bar{3}m$). The phonon analysis of PVDF-$BaTiO_3$-3% nanofibrous composite by Raman scattering is shown in Figure 5. For the $BaTiO_3$ with tetragonal symmetry ($P4mm$, C_{4v}), the broad peak centered near 259 cm^{-1} [$A_1(2TO)$], a sharp peak at 307 cm^{-1} [B_1+E(2LO)+E(3TO)], an asymmetric and broad peak near 514 cm^{-1} [(3TO)+E(4TO)] and a weak peak around 719 cm^{-1} [(3LO)+E(4LO)] where the phonon assignment is given inside square brackets [37, 38, 39]. It can be concluded that $BaTiO_3$ exists in tetragonal structure in the electrospun composite.

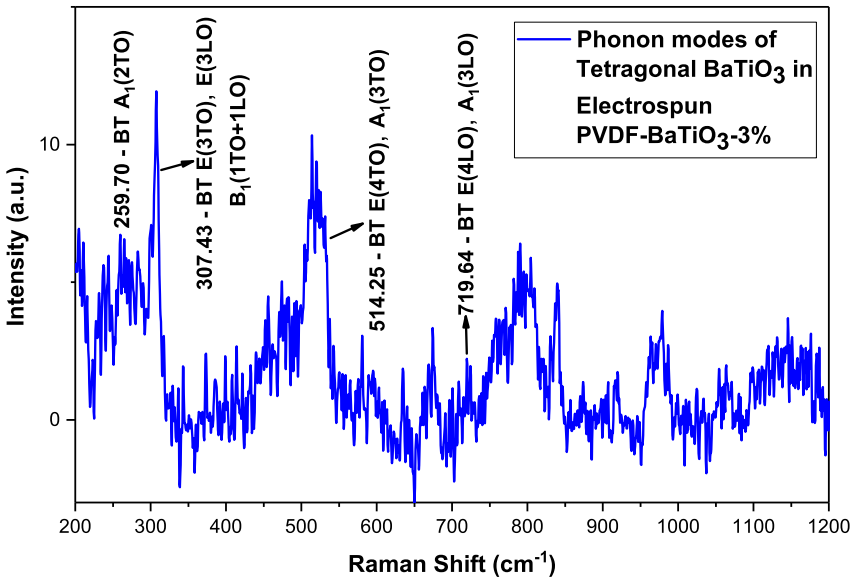

Figure 5: Raman spectra of PVDF-$BaTiO_3$-3% nanofibrous composite.

It was found that, the intensity of Raman modes of $BaTiO_3$ gradually decrease compared to as received Raman spectrum of powdered $BaTiO_3$ (provided by the manufacturer (Sigma-Aldrich)). This is due to ultrasonication process which causes the particle size reduction and defects creation. The average size of particles obtained

from sigma-aldrich was ≈ 3 μm, which is expected to reduce further in size due to ultrasonication. In addition to defects creation, the ultrasonic acoustic waves also create lattice distortions leading to stabilized distorted tetragonal structure in the electrospun composite.

5.3. Crystalline phases of electrospun fibers

Among the different polymorphs of PVDF including the α-phase, β-phase γ-phase δ-phase and ϵ- phase, the α-phase has a monoclinic structure and is a dominant phase which is non-polar in nature. Except the α-phase, all other phases are electroactive in nature and possess a net dipole moment. The β-phase and γ-phase has a orthorhombic crystal structure. Among the electroactive phases, the β-phase is desired because it has a large dielectric constant. The higher dielectric constant/relative permittivity (ε_r) is due to fluorine, an electronegative element present in all-trans (ttttt) chain conformation leading to large spontaneous polarization of the electron cloud. The orientation of the fluorine atom determines the phase that will form among four different polymorphs in fabrication.

The most common and stable α-phase is produced by crystallization from the melt or solution. The α-phase can be transformed into the polar form, the β-phase, by mechanically stretching or rolling at elevated temperatures. Since all the dipole moments become perpendicular to the chain axes, microscopically, each crystallite has a net dipole moment and exhibits piezoelectric behavior. However, on the macroscopic scale, there is no polarization within the polymer due to the random orientation of the dipole moments of the crystallites. To render the PVDF film piezoelectric, a highly aligned β-phase PVDF is required. However producing a β-phase PVDF poses a challenge, requiring additional processing techniques such as poling/mechanical stretching. Poling involves the application of an electric field. This step preferentially aligns the dipoles of the crystallites in the direction of the applied electric field and thus produces a net polarization. The two main poling techniques are conventional two-electrode poling (also referred to as thermal poling) and corona poling. Compared to these processes, the inexpensive electrospinning process [40] offers a unique methodology to prepare the nanofibers by preserving the semi-crystalline nature of the polymer and also aid in producing the β-phase content in the PVDF due to high applied voltage, which causes the polarization of electron cloud around the fluorine atom.

The FT-IR spectra of all the investigated electrospun samples of PVDF and PVDF-$BaTiO_3$-3% nanofibrous composite are shown in Figure 6. The peak values and fingerprint regions are assigned in Table 2. It has been previously reported [41] that the β-phase absorption band is at 1278 cm^{-1}. The peak at 1278 cm^{-1} in Figure 6 indicates the β-phase formation by the electrospinning process. The analysis shows the presence of both α and β phases in the semi-crystalline PVDF fibrous mats. The addition of $BaTiO_3$ to the PVDF causes the intensity of β-phase peak to increase. The added $BaTiO_3$ particles induces the PVDF polymer to crystallize in a more polar β-phase

PVDF during the electrospinning process as reported in [42]. Hence, the electrospinning process offers a cost-effective and synergistic approach combining electrode poling and mechanical stretching to produce PVDF nanofibers with β-phase content.

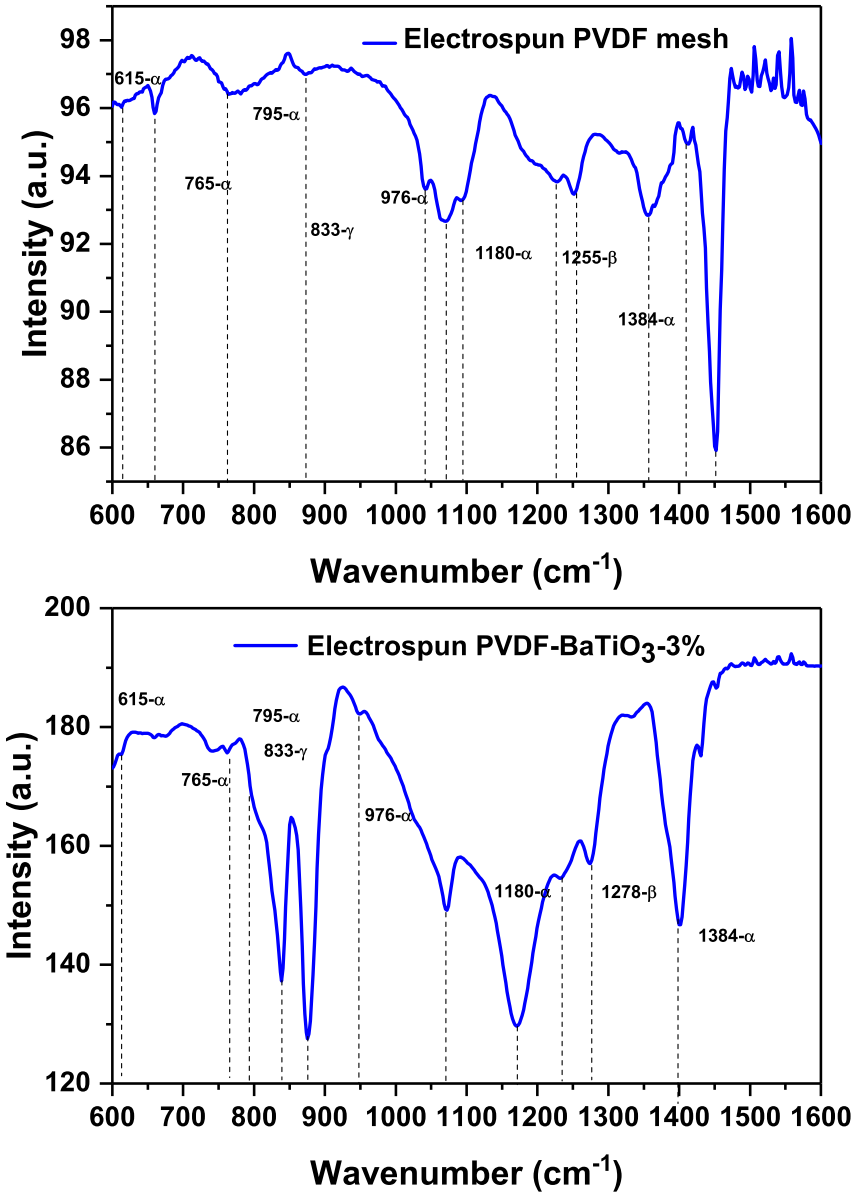

Figure 6: FTIR spectra of PVDF and the PVDF-$BaTiO_3$-3% nanofibrous composite - a) Electrospun PVDF mesh b) PVDF-$BaTiO_3$-3% nanofibrous composite mesh.

The FT-IR spectrum of PVDF powder (CAS Number 24937-79-9) provided by sigma-aldrich was examined for the beta phase content. Although, a small shoulder of a peak at $\approx$ 1278 cm^{-1} corresponding to β-phase was identified, it predominantly had α-phase. When the FT-IR spectrum of electrospun sample was compared, the peak intensity at $\approx$ 1255 cm^{-1} - 1278 cm^{-1} was found to increase implying that the

Table 2: Characteristics Infra-red vibration modes of PVDF and PVDF-$BaTiO_3$-3% nanofibrous composite.

Wavenumber, cm^{-1}	Vibration mode	Phase	Ref.
615	CF_2 bending	α-phase	[43, 44, 45]
765	In-plane bending/rocking	α-phase	[44]
836	CH_2 out of plane wagging	β-phase	[46]
881	CH_2 rocking vibrations	β-phase	[46]
976		α-phase	[43]
1050	CF stretching vibration		[47]
1060	CF stretching vibration		[47]
1090	CF stretching vibration		[47]
1180	CF stretching vibration		[47]
1234		γ-phase	[43]
1278		β-phase	[43]
1403	CH_2 Scissoring	β-phase	[46]
1452	CH_2/Ti–O Scissoring/vibrations		[46]
1453	CH_2 In-plane bending/scissoring		[48]

electrospinning process does increase the beta phase content in the polymer due to the applied electric field of 20 kV during electrospinning process. To further verify the result, a compression molded sample was prepared with PVDF and PVDF-$BaTiO_3$-3% and subjected to phonon analysis by Raman scattering along with electrospun samples as described in the following section.

5.4. Phonon analysis by Raman scattering

The addition of the $BaTiO_3$ particles along with the electrospinning process promotes β-phase crystallization over α-phase crystallization. It can be seen in Figure 7 that the intensity of the sharp peak around ≈ 795 cm^{-1} corresponding alpha phase is significantly reduced in the electrospun fibrous samples compared to compression molded samples. At the same time, an increase in peak intensity was observed around $\approx$ 839 cm^{-1} corresponding to beta phase. The γ-phase around ≈ 810 cm^{-1} also found to increase in electrospun samples. Along with FTIR analysis, Raman scattering analysis further proves the increase in beta phase content by the addition of $BaTiO_3$ and electrospinning process.

5.5. Adhesion property

The electrospun fibers usually have a high aspect ratio, leading to large surface area when compared with conventional fibers [49]. Due to this property, electrospun fibers find use in various applications. On the nanoscale level, the β-phase is found to decrease the adhesion force, because of less electrostatic force in β-phase compared to the α and γ phases [50]. Adhesion type Electromagnetic acoustic transducers (EMAT) are used

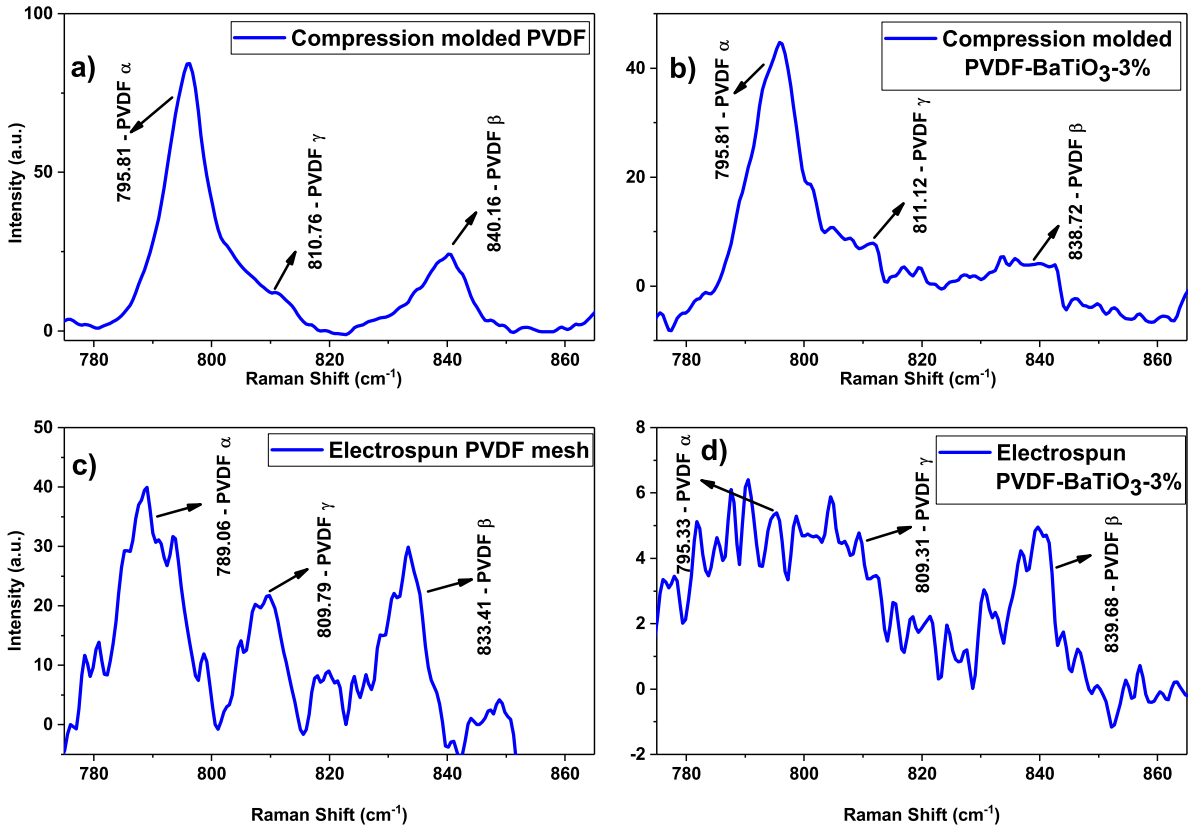

Figure 7: Raman spectra of PVDF and the PVDF-$BaTiO_3$-3% nanofibrous composite - a) Compression molded PVDF b) Compression molded PVDF-$BaTiO_3$-3% c) Electrospun PVDF mesh d) PVDF-$BaTiO_3$-3% nanofibrous composite mesh.

for structural health monioring applications where a couplant is not used between the sensor and structural member to be monitored [51]. This type of sensors improve the efficiency of receiving elastic waves which are generated due to defects in structural members under constant loading conditions. The electrospun PVDF-$BaTiO_3$-3% mats can have different adhesive property compared to thin polymer film owing to its oriented fibrous structure. The addition of 3% $BaTiO_3$ produces a finer nanofibrous mesh, Due to this, the adhesion property of the fibrous materials can be enhanced.

The water contact angle for PVDF fibrous mesh was 80° (Figure 8a). The PVDF-$BaTiO_3$-3% composite mesh has the water contact angle of 90° (Figure 8b) making it more hydrophobic. The addition of $BaTiO_3$ to the PVDF fibers causes it to become more hydrophobic with higher sticking tendency towards the structural member. This kind of anisotropic wetting behavior can be attributed to both structural and chemical gradients on the surface [52]. Although, the β-phase content tends to decrease the electrostatic force on the surface [50], the reduction in fiber diameter in case of PVDF-$BaTiO_3$-3% composite causes water contact angle to increase. So, the mesoscale property of morphology contributes more to the adhesion property than the nano scale chemical

elements present in the structure.

The electrospinning process has a potential to produce nanoscale polymer fibers with a simple and cost effective process. The high productivity, reproducibility and a potential to be scaled up to the industrial scale [53, 54] make the electrospinning process an attractive technique to proudce fibrous material for EMAT sensing and dry adhesive applications [55].

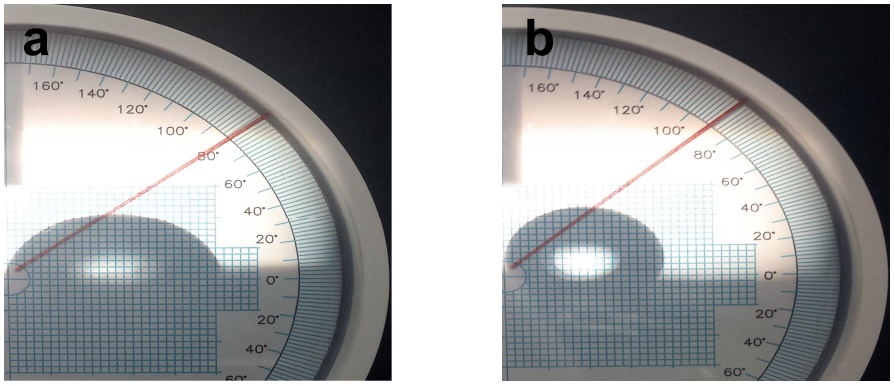

Figure 8: Water contact angle of a) electrospun PVDF nanofibers and b) electrospun PVDF-$BaTiO_3$-3% nanofibrous composite.

5.6. Capacitance

The capacitance of the dielectric material in a parallel plate configuration can be calculated using the following equation:

$$C(\omega) = \varepsilon_0 \, \varepsilon^{'}(\omega) \frac{A}{d} \tag{5.6.1}$$

In the above equation, $C(\omega)$ is capacitance, ω is angular frequency, A is sample's cross-sectional area (491.07 mm^2), d is thickness of the sample which is 0.55 mm. ε_0 is permittivity of free space which is equal to 8.854 pF/m. $\varepsilon^{'}(\omega)$ is frequency dependent dielectric permittivity measured from experiment. The calculated frequency dependent capacitance values are plotted in Figure 9.

The increase in capacitance value of polymer composite can be attributed to the presence of $BaTiO_3$ in the nanofibrous composite. The cubic crystal structure with a lattice constant of 4.01 Å exists above its Curie temperature of 120°C, below this temperature it converts to the tetragonal form with unequal side lengths: 3.98 Å and 4.03 Å, thereby with existence of permanent dipole moments causing the mobile ionic charge resulting in spontaneous polarization and a higher dielectric constant (κ) value of $\approx$ 400-450. However, very high processing temperature above 600°C is required for sintering of these materials to process them into desired shape, which make them unsuitable to process with polymer materials, because polymer materials become unstable at these very high temperatures. This issue can be overcome by making use

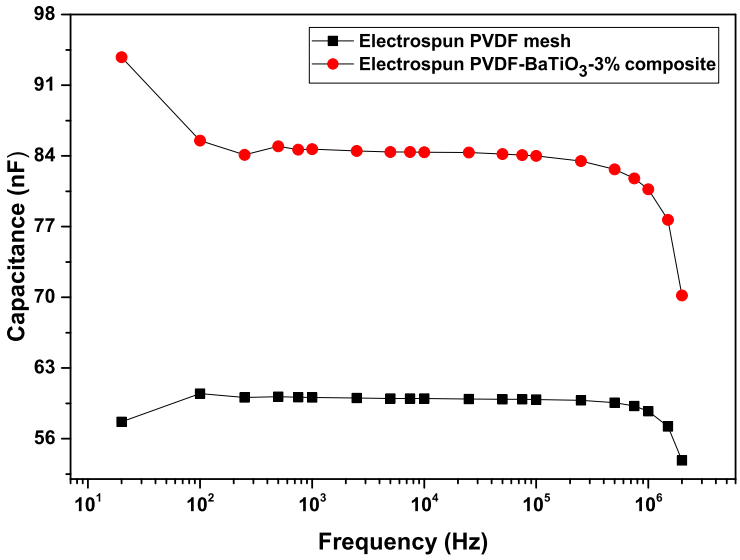

Figure 9: Variation of Capacitance with respect to frequency.

of flexible polymer composites in which $BaTiO_3$ particles can be used as fillers for fabricating sensors of complex shapes.

6. Conclusion

A dielectric polyvinylidene fluoride (PVDF) and PVDF-$BaTiO_3$-3% nano-fibrous composites were made using electrospinning process. A 2^k factorial DoE approach was used to optimize the filler concentration and ultrasonication process for fabricating the nanofibrous composite. Scanning electron microscopy was used to characterize the microstructure of the fabricated mesh. The results obtained indicates the DoE approach is an efficient method to optimize the filler concentration and thereby fiber morphology. FT-IR and Raman spectroscopic analysis revealed the formation of polarized β-phase crystal structure in the electrospun fibers by the addtion of tetragonal $BaTiO_3$ and the electrospinning process. The electrospun PVDF-$BaTiO_3$-3% mats can have different adhesive property compared to thin polymer film prepared by spin coating, owing to its oriented fibrous structure resempling gecko feet. The addition of $BaTiO_3$-3% produces a finer nanofibrous mesh. Due to this, the adhesion property of the fibrous materials can be enhanced. The capacitance of the PVDF and PVDF-$BaTiO_3$-3% composite were calculated from dielectric measurements and found a 40% increase in capacitance value for the PVDF-$BaTiO_3$-3% nanofibrous composite compared to PVDF nanofibers. Hence making nanofibrous material using electrospinning process is an efficient and cost-effective way to prepare materials mimicking biological skin to have increased surface adhesion. The prepared material can find potential application as flexible piezoelctric/capacitive sensor for structural health monitoring applications. The 2^k

factorial DoE approach will be useful for fabricating electrospun nanofibrous composite materials with large particle size fillers.

7. Acknowledgments

The author would like to acknowledge Mechanical and energy engineering department and Materials research facility at University of North Texas for fabrication and characterization of materials.

8. References

References

[1] Ishida H, Campbell S and Blackwell J 2000 *Chemistry of Materials* **12** 1260–1267 URL https://doi.org/10.1021/cm990479y

[2] Chiang C K and Popielarz R 2002 *Ferroelectrics* **275** 1–9 ISSN 0015-0193 URL http://www.tandfonline.com/doi/abs/10.1080/00150190214285

[3] Li M, Zhang J, Zhang H, Liu Y, Wang C, Xu X, Tang Y and Yang B 2007 *Advanced Functional Materials* **17** 3650–3656 ISSN 1616301X URL http://doi.wiley.com/10.1002/adfm.200700241

[4] Dror Y, Salalha W, Khalfin R L, Cohen Y, Yarin A L and Zussman E 2003 *Langmuir* **19** 7012–7020 ISSN 0743-7463 URL http://dx.doi.org/10.1021/la034234i

[5] Biswas S and Drzal L T 2010 *Chemistry of Materials* **22** 5667–5671 ISSN 0897-4756 URL http://dx.doi.org/10.1021/cm101132g

[6] Nalwa H S 1995 *Ferroelectric polymers : chemistry, physics, and applications* (New York City: M. Dekker, Inc) ISBN 9780824794682 URL https://www.crcpress.com/Ferroelectric-Polymers-Chemistry-Physics-and-Applications/Nalwa/p/book/9780824794682

[7] Sahay R, Kumar P S, Sridhar R, Sundaramurthy J, Venugopal J, Mhaisalkar S G and Ramakrishna S 2012 *Journal of Materials Chemistry* **22** 12953 ISSN 0959-9428 URL http://xlink.rsc.org/?DOI=c2jm30966a

[8] Li Y, Yu J and Ding B 2015 Facile and Ultrasensitive Sensors Based on Electrospinning-Netting Nanofibers/Nets. in *Electrospinning for High Performance Sensors* ed Macagnano A, Zampetti E and Kny E (Cham: Springer) chap 1, pp 1–34 ISBN 978-3-319-14405-4 URL http://link.springer.com/10.1007/978-3-319-14406-1

[9] Yun J S, Park C K, Jeong Y H, Cho J H, Paik J H, Yoon S H and Hwang K R 2016 *Nanomaterials and Nanotechnology* **6** 20 ISSN 1847-9804 URL http://journals.sagepub.com/doi/10.5772/62433

[10] Laflamme S, Kollosche M, Connor J J and Kofod G 2013 *Journal of Engineering Mechanics* **139** 879–885 ISSN 0733-9399 URL http://ascelibrary.org/doi/abs/10.1061/(ASCE)EM.1943-7889.0000530

[11] Mendes S F, Costa C M, Caparros C, Sencadas V and Lanceros-Méndez S 2012 *Journal of Materials Science* **47** 1378–1388 ISSN 0022-2461 URL http://link.springer.com/10.1007/s10853-011-5916-7

[12] Olmos D, Gonzalez-Gaitano G, Vela R, Cordoba L, Gonzalez-Benito J and Kholkin A L 2012 Flexible PVDF-BaTiO3 nanocomposites for pressure sensors *Proceedings of ISAF-ECAPD-PFM 2012* (Aveiro, Portugal: IEEE) pp 1–3 ISBN 978-1-4673-2669-8 URL http://ieeexplore.ieee.org/document/6297828/

[13] Sánchez-Jiménez P E, Pérez-Maqueda L A, Diánez M J, Perejón A and Criado J M 2010 *Composite Structures* **92** 2236–2240 ISSN 0263-8223 URL https://www.sciencedirect.com/science/article/pii/S026382230900289X

[14] Zheng P, Zhang J, Tan Y and Wang C 2012 *Acta Materialia* **60** 5022–5030 ISSN 1359-6454 URL https://www.sciencedirect.com/science/article/pii/S1359645412003771

[15] Najem J F, Wong S C and Ji G 2014 *Langmuir* **30** 10410–10418 ISSN 0743-7463 URL http://pubs.acs.org/doi/10.1021/la502402y

[16] Naghieh S, Foroozmehr E, Badrossamay M and Kharaziha M 2017 *Materials & Design* **133** 128–135 ISSN 0264-1275 URL https://www.sciencedirect.com/science/article/pii/S0264127517307207

[17] Jarusuwannapoom T, Hongrojjanawiwat W, Jitjaicham S, Wannatong L, Nithitanakul M, Pattamaprom C, Koombhongse P, Rangkupan R and Supaphol P 2005 *European Polymer Journal* **41** 409–421 ISSN 00143057 URL http://www.sciencedirect.com/science/article/pii/S0014305704003684

[18] Taurozzi J, Hackley V and Wiesner M 2012 Preparation of Nanoparticle Dispersions from Powdered Material Using Ultrasonic Disruption - Version 1.1 Tech. rep. NIST Gaithersburg, MD URL https://nvlpubs.nist.gov/nistpubs/SpecialPublications/NIST.SP.1200-2.pdf

[19] Yördem O, Papila M and Menceloğlu Y 2008 *Materials & Design* **29** 34–44 ISSN 0261-3069 URL https://www.sciencedirect.com/science/article/pii/S0261306906003967

[20] Cui W, Li X, Zhou S and Weng J 2007 *Journal of Applied Polymer Science* **103** 3105–3112 ISSN 00218995 URL http://doi.wiley.com/10.1002/app.25464

[21] Ruiter F A A, Alexander C, Rose F R A J and Segal J I 2017 *Biomedical Materials* **12** 055009 ISSN 1748-605X URL http://stacks.iop.org/1748-605X/12/i=5/a=055009?key=crossref.ddb783219cc86304d1d55211d83cde62

[22] R Core Team 2018 *R: A Language and Environment for Statistical Computing* R Foundation for Statistical Computing Vienna, Austria URL https://www.R-project.org/

[23] Grömping U 2018 *Journal of Statistical Software, Articles* **85** 1–41 ISSN 1548-7660 URL https://www.jstatsoft.org/v085/i05

[24] Sigmund P 1969 *Physical Review* **184** 383–416 ISSN 0031-899X URL http://journals.aps.org/pr/abstract/10.1103/PhysRev.184.383

[25] Schneider C A, Rasband W S and Eliceiri K W 2012 *Nature Methods* **9** 671–675 ISSN 1548-7091 URL http://www.nature.com/articles/nmeth.2089

[26] Zong X, Kim K, Fang D, Ran S, Hsiao B S and Chu B 2002 *Polymer* **43** 4403–4412 ISSN 00323861 URL http://www.sciencedirect.com/science/article/pii/S0032386102002756

[27] Schümmer P and Tebel K 1983 *Journal of Non-Newtonian Fluid Mechanics* **12** 331–347 ISSN 03770257 URL http://www.sciencedirect.com/science/article/pii/037702578385006X

[28] Megelski S, Stephens J S, Chase D B and Rabolt J F 2002 *Macromolecules* **35** 8456–8466 ISSN 0024-9297 URL http://dx.doi.org/10.1021/ma020444a

[29] Fong H 2004 *Polymer* **45** 2427–2432 ISSN 00323861 URL http://www.sciencedirect.com/science/article/pii/S0032386104001156

[30] Zhao S, Wu X, Wang L and Huang Y 2004 *Journal of Applied Polymer Science* **91** 242–246 ISSN 0021-8995 URL http://doi.wiley.com/10.1002/app.13196

[31] Demir M, Yilgor I, Yilgor E and Erman B 2002 *Polymer* **43** 3303–3309 ISSN 00323861 URL http://www.sciencedirect.com/science/article/pii/S0032386102001362

[32] Mo X, Xu C, Kotaki M and Ramakrishna S 2004 *Biomaterials* **25** 1883–1890 ISSN 01429612 URL http://www.sciencedirect.com/science/article/pii/S0142961203006951

[33] Taurozzi J S, Hackley V A and Wiesner M R 2011 *Nanotoxicology* **5** 711–729 ISSN 1743-5390 URL http://www.tandfonline.com/doi/full/10.3109/17435390.2010.528846

[34] Mohamed-Noriega N, Hinojosa M, González V and Rodil S E 2016 *Optical Materials* **58** 18–23 ISSN 0925-3467 URL https://www.sciencedirect.com/science/article/pii/S092534671630146X

[35] Cho W S and Hamada E 1998 *Journal of Alloys and Compounds* **266** 118–122 ISSN 0925-8388 URL http://www.sciencedirect.com/science/article/pii/S0925838897004465

[36] Noma T, Wada S, Yano M and Suzuki T 1998 *Journal of Applied Physics* **80** 5223 ISSN 0021-8979 URL https://aip.scitation.org/doi/10.1063/1.363508

[37] Venkateswaran U D, Naik V M and Naik R 1998 *Phys. Rev. B* **58** 14256–14260 URL https://link.aps.org/doi/10.1103/PhysRevB.58.14256

[38] Hoshina T, Kakemoto H, Tsurumi T, Wada S and Yashima M 2006 *Journal of Applied Physics* **99** 054311 ISSN 0021-8979 URL http://aip.scitation.org/doi/10.1063/1.2179971

[39] Pavlović V P, Pavlović V B, Vlahović B, Božanić D K, Pajović J D, Dojčilović R and Djoković V 2013 *Physica Scripta* **T157** 014006 ISSN 0031-8949 URL http://stacks.iop.org/1402-4896/2013/i=T157/a=014006?key=crossref.2e1abea69d3688a183a8ec27228e39c0

[40] Andrew J S and Clarke D R 2008 *Langmuir* **24** 670–672 URL https://doi.org/10.1021/la7035407

[41] Gregorio R 2006 *Journal of Applied Polymer Science* **100** 3272–3279 ISSN 0021-8995 URL http://doi.wiley.com/10.1002/app.23137

[42] Chanmal C V and Jog J P 2011 *International Journal of Plastics Technology* **15** 1–9 ISSN 0972-656X URL http://link.springer.com/10.1007/s12588-011-9001-5

[43] Martins P, Lopes A and Lanceros-Mendez S 2014 *Progress in Polymer Science* **39** 683–706 ISSN 0079-6700 URL https://www.sciencedirect.com/science/article/pii/S0079670013000865

[44] Betz N, Le Moël A, Balanzat E, Ramillon J M, Lamotte J, Gallas J P and Jaskierowicz G 1994 *Journal of Polymer Science Part B: Polymer Physics* **32** 1493–1502 ISSN 08876266 URL http://doi.wiley.com/10.1002/polb.1994.090320821

[45] Mattsson B, Ericson H, Torell L and Sundholm F 2000 *J. Polym. Sci. A Polym. Chem.* **37** 3317–3327 URL https://onlinelibrary.wiley.com/doi/abs/10.1002/%28SICI%291099-0518%2819990815%2937%3A16%3C3317%3A%3AAID-POLA30%3E3.0.CO%3B2-%23

[46] Gaur M S, Singh P K, Ali A and Singh R 2014 *Journal of Thermal Analysis and Calorimetry* **117** 1407–1417 ISSN 1388-6150 URL http://link.springer.com/10.1007/s10973-014-3908-y

[47] Lanceros-Méndez S, Mano J F, Costa A M and Schmidt V H 2001 *Journal of Macromolecular Science, Part B* **40** 517–527 ISSN 0022-2348 URL http://www.tandfonline.com/doi/abs/10.1081/MB-100106174

[48] Silverstein R M R M, Webster F X, Kiemle D J and Bryce D L D L 1962 *Spectrometric identification of organic compounds* 8th ed (Hoboken, NJ, USA: John Wiley & Sons) ISBN 0470616377 URL https://www.wiley.com/en-us/Spectrometric+Identification+of+Organic+Compounds%2C+8th+Edition-p-9780470616376

[49] Ramakrishna S, Fujihara K, Teo W E, Lim T C and Ma Z 2005 *An Introduction to Electrospinning and Nanofibers* (Hackensack, NJ: WORLD SCIENTIFIC) ISBN 978-981-256-415-3 URL http://www.worldscientific.com/worldscibooks/10.1142/5894

[50] Jee T, Lee H, Mika B and Liang H 2007 *Tribology Letters* **26** 125–130 ISSN 1023-8883 URL http://link.springer.com/10.1007/s11249-006-9163-z

[51] Tone R, Tanaka Y and Fujimoto Y 2014 *International Journal of Applied Electromagnetics and Mechanics* **45** 171–177

ISSN 1383-5416 URL https://content.iospress.com/articles/international-journal-of-applied-electromagnetics-and-mechanics/jae01827

[52] Xia D, Johnson L M and López G P 2012 *Advanced Materials* **24** 1287–1302 ISSN 09359648 URL http://doi.wiley.com/10.1002/adma.201104618

[53] Heikkila, P and Harlin A 2009 *eXPRESS Polymer Letters* **3** 437–445 URL https://doi.org/10.3144/expresspolymlett.2009.53

[54] Fong H, Chun I and Reneker D 1999 *Polymer* **40** 4585–4592 ISSN 00323861 URL http://www.sciencedirect.com/science/article/pii/S0032386199000683

[55] Sahay R, Parveen H, Baji A, Ganesh V A and Ranganath A S 2017 *Journal of Materials Science* **52** 2435–2441 ISSN 0022-2461 URL http://link.springer.com/10.1007/s10853-016-0537-9